Influence of Hydrophobic Mismatch on Structures and Dynamics of Gramicidin A and Lipid Bilayers

Taehoon Kim,[†] Kyu Il Lee,[†] Phillip Morris,[†] Richard W. Pastor,[‡] Olaf S. Andersen,[§*] and Wonpil Im[†*]
[†]Department of Molecular Biosciences and Center for Bioinformatics, The University of Kansas, Lawrence, Kansas; [‡]Laboratory of Computational Biology, National Heart, Lung, and Blood Institute, National Institutes of Health, Bethesda, Maryland; and [§]Department of Physiology and Biophysics, Weill Cornell Medical College, New York, New York

ABSTRACT Gramicidin A (gA) is a 15-amino-acid antibiotic peptide with an alternating L-D sequence, which forms (dimeric) bilayer-spanning, monovalent cation channels in biological membranes and synthetic bilayers. We performed molecular dynamics simulations of gA dimers and monomers in all-atom, explicit dilauroylphosphatidylcholine (DLPC), dimyristoylphosphatidylcholine (DMPC), dioleoylphosphatidylcholine (DOPC), and 1-palmitoyl-2-oleoyl-phosphatidylcholine (POPC) bilayers. The variation in acyl chain length among these different phospholipids provides a way to alter gA-bilayer interactions by varying the bilayer hydrophobic thickness, and to determine the influence of hydrophobic mismatch on the structure and dynamics of both gA channels (and monomeric subunits) and the host bilayers. The simulations show that the channel structure varied little with changes in hydrophobic mismatch, and that the lipid bilayer adapts to the bilayer-spanning channel to minimize the exposure of hydrophobic residues. The bilayer thickness, however, did not vary monotonically as a function of radial distance from the channel. In all simulations, there was an initial decrease in thickness within 4–5 Å from the channel, which was followed by an increase in DOPC and POPC or a further decrease in DLPC and DMPC bilayers. The bilayer thickness varied little in the monomer simulations—except one of three independent simulations for DMPC and all three DLPC simulations, where the bilayer thinned to allow a single subunit to form a bilayer-spanning water-permeable pore. The radial dependence of local lipid area and bilayer compressibility is also nonmonotonic in the first shell around gA dimers due to gA-phospholipid interactions and the hydrophobic mismatch. Order parameters, acyl chain dynamics, and diffusion constants also differ between the lipids in the first shell and the bulk. The lipid behaviors in the first shell around gA dimers are more complex than predicted from a simple mismatch model, which has implications for understanding the energetics of membrane protein-lipid interactions.

INTRODUCTION

Membrane protein function is in part regulated by changes in lipid bilayer thickness and intrinsic lipid curvature (1). This regulation of membrane protein function arises because the energetic penalty for exposure of hydrophobic residues to water, between 25 and 75 cal/(mol · Å^2) (2), causes the protein and bilayer adapt to each other (3). Changes in protein conformation that involve the protein's transmembrane (TM) domain therefore will cause local changes in lipid packing. In the case of a hydrophobic mismatch (between the length of a protein's hydrophobic TM domain and the thickness of the bilayer hydrophobic core), the bilayer adaptation involves local changes in lipid bilayer thickness, and possibly changes in TM domain orientation. Focusing on the changes in bilayer organization, the local bilayer thickness change (protein-induced bilayer deformation) has an associated energetic cost, the bilayer deformation energy (ΔG_{def}) (4,5). The difference in ΔG_{def} associated with two different conformations (I and II) of the protein of interest is the bilayer contribution to the free energy difference for the conformational transition, $\Delta G^{I\rightarrow II}_{bilayer} = \Delta G^{II}_{def} - \Delta G^{I}_{def}$ (3).

ΔG_{def} can be evaluated using the theory of elastic bilayer deformations (5–10). The theory has been calibrated using changes in gramicidin A (gA) single-channel lifetimes (τ) as a function of bilayer thickness (d_0) (5,11), and changes in gA channel appearance rate (f) and τ as a function of membrane tension (σ) (12). These studies form the most comprehensive test available of the theory, and the results show that ΔG_{def} varies as a function of the boundary conditions for lipid packing at the protein/bilayer boundary (6,8,9). In addition, the f-σ and τ-σ relations (12) and τ-d_0 relation (11) for gA channels do not conform to predictions based on the elastic bilayer model using bulk bilayer elastic moduli and boundary conditions that minimize ΔG_{def}. The experimental results could be fit by varying the slope (s) of the bilayer/solution interface at the channel/bilayer boundary. This indicates that there are additional constraints on lipid packing, for example the energetic cost of acyl-chain tilt (8), which would tend to move s toward 0. Indeed, the τ-d_0 relation could be fit by assuming $s = 0$ (11). Alternatively, the bilayer elastic moduli close to the channel could be larger than the bulk moduli (10), or there might be additional constraints on the local lipid packing. These modifications of the basic elastic bilayer model would be compatible with the τ-d_0 results, but constraining s to be 0 is difficult to reconcile with the observed effects of varying the intrinsic curvature (3,9,13).

To obtain insight into the preceding problems and to understand how a channel-bilayer hydrophobic mismatch alters the local lipid structure and dynamics, we used

Submitted November 20, 2011, and accepted for publication March 5, 2012.

*Correspondence: sparre@med.cornell.edu or wonpil@ku.edu

Editor: Scott Feller.

0006-3495/12/04/1551/10 $2.00

doi: 10.1016/j.bpj.2012.03.014

molecular dynamics (MD) simulation to explicitly probe the radial bilayer deformation profile around bilayer-spanning gA channels and evaluate the lipid fluctuations, which allows for the determination of local compressibility moduli. The radial dependence of lipid organization and dynamics were not extensively investigated in previous MD simulations of gA channels in lipid bilayers (14,15) because the number of lipid molecules was insufficient (usually 10 lipids/gA monomer, or one shell) to explore gA-lipid bilayer interactions that might propagate over several shells. To explore the influence of hydrophobic mismatch on the structure and dynamics of gA bilayer-spanning dimers and monomeric subunits, as well as the lipids in the vicinity of the channel or subunit, we therefore performed MD simulations of gA dimers and monomers embedded in single-component phosphatidylcholine bilayers of different thickness—dilauroylphosphatidylcholine (DLPC), dimyristoylphosphatidylcholine (DMPC), dioleoylphosphatidylcholine (DOPC), and 1-palmitoyl-2-oleoyl-phosphatidylcholine (POPC) bilayers, each with four lipid shells around the dimer or monomer.

The influence of hydrophobic mismatch on the structure and dynamics of gA bilayer-spanning dimers and monomeric subunits were characterized in terms of the root mean-squared deviation (RMSD), hydrogen-bonding patterns, orientation (tilt and rotation), Trp side chain orientation, and relative positions in bilayers. We also calculated key lipid properties such as hydrophobic thickness, per-lipid surface area, compressibility, acyl chain order parameter, and lateral diffusion coefficient, as functions of radial distance from the channel, and discuss them in terms of the influence of hydrophobic mismatch on lipid bilayer structure and dynamics and the energetic coupling between integral membrane proteins and their host bilayers.

METHODS

Using the Membrane Builder module (16,17) in CHARMM-GUI (www.charmm-gui.org) (18), the gA dimer structure from PDB:1JNO (19) with added pore water molecules was inserted into four different lipid bilayers with 180 DLPC, DMPC, DOPC or POPC molecules, which corresponds to approximately four lipid shells around the channel. For the simulation on the gA monomers, a monomeric subunit from the gA dimer was inserted into one leaflet and five more lipid molecules were added into the other leaflet. 0.15 M KCl was used for all simulations. Each system was replicated and assigned different initial velocities to generate three independent simulation systems for each type of lipid bilayer, yielding a total of 24 systems. Table S1 in the Supporting Material summarizes the system information (see also Fig. 1).

All calculations were performed in the NPT (constant particle number, pressure, and temperature) ensemble (20) at 303.15 K using CHARMM (21) with the CHARMM all-atom protein force field (22) including a modified version of dihedral cross-term correction (referred to as "dCMAP") (23,24), the CHARMM36 lipid force field (25), and a modified TIP3 water model (26). A time-step of 2 fs was used with the SHAKE algorithm (27).

Each initial system was equilibrated using 50-ps NPAT (constant particle number, pressure, *XY* area, and temperature) dynamics followed by 325-ps NPT dynamics with the nonbonded and dynamics options in the Membrane Builder input; the van der Waals interactions were smoothly switched off at 10–12 Å by a force-switching function (28) and the electrostatic interactions were calculated using the particle-mesh Ewald method (29) with a mesh size of ~1 Å for fast Fourier transformation, $\kappa = 0.34$ Å^{-1}, and a sixth-order B-spline interpolation. After equilibration, a 100-ns production run was performed for each system.

RESULTS AND DISCUSSION

Influence of hydrophobic mismatch on gA structure and dynamics

Both the bilayer-spanning dimers (channels) and the monomeric subunits were stable for the duration of the simulations. The RMSD from the PDB:1JNO structure for the dimers were less than those for the monomers (Fig. 2 *A*),

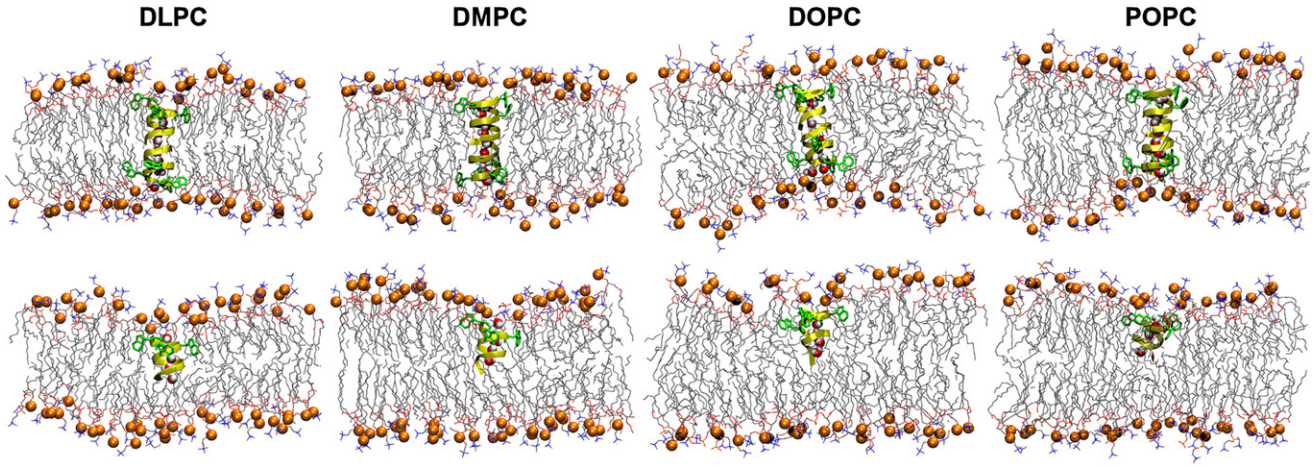

FIGURE 1 Snapshots of gramicidin (gA) dimers (*top*) and monomers (*bottom*) in DLPC, DMPC, DOPC, and POPC bilayers. Coordinate sets are from 100-ns time point of the trajectories with the exception of the monomer in DLPC; as described later, this system formed water-permeable pores, so a prepore (45 ns) snapshot is shown. (*Yellow*) gA dimers and monomers; (*green*) Trp residues; (*gray*) lipid carbons. (*Spheres*) Pore water molecules; (*orange spheres*) lipid phosphate; bulk water and ions are omitted for clarity.

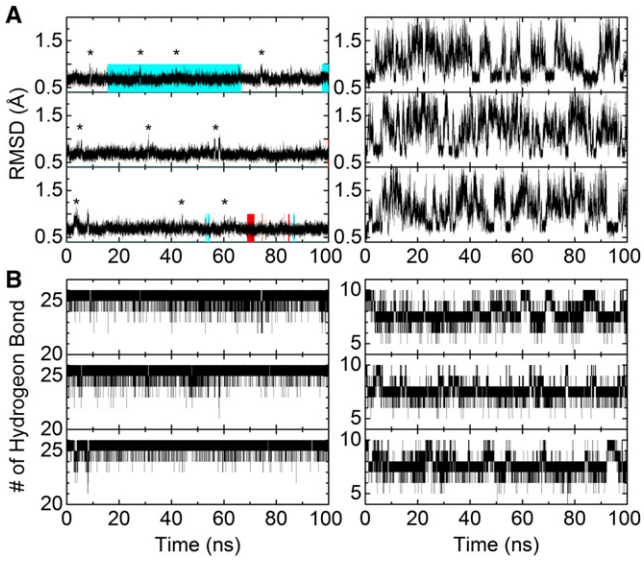

FIGURE 2 (*A*) RMSD time series for a gA dimer (*left*) and the monomeric subunit (*right*) in a DOPC bilayer. Cyan and red colored regions represent the binding of K^+ at the upper (*cyan*) and lower (*red*) pore entrances. Ethanolamide (EAM) swing motions are marked by an asterisk (*). (*B*) The number of hydrogen bonds in the dimer (*left*) and the monomeric subunit (*right*) in a DOPC bilayer. Fig. S1 shows the results from the DLPC, DMPC, and POPC bilayer simulations.

reflecting that the intersubunit hydrogen bonds stabilize the subunit structure. The number of hydrogen bonds in the dimers (Fig. 2 *B*) mostly varied between 22 and 26 (the maximum possible), with an average of 25 and occasional transitions to lower numbers. Except in the DOPC bilayers, we observed transient increases in the RMSD for the dimers; these increases were correlated with the loss of hydrogen bonds that were usually caused by one of ethanolamide (EAM) termini swinging out from the channel (24) (see Fig. S1 in the Supporting Material). K^+ binding to the carbonyl oxygens at the channel entrance also caused slight increases of the dimer RMSD. The number of hydrogen bonds in the monomers mostly varied between 6 and 10 (the maximum possible), with an average of 8 and occasional transitions to lower numbers. The average number of residues per turn was 6.28–6.29 (compared to 6.3 in the PDB:1JNO structure (19)); the average rise per turn was 4.51–4.57 Å (compared to 4.7 ± 0.2 Å in PDB:1JNO and also deduced from x-ray diffraction (30)). There are no significant differences among the dimer structures in different lipid bilayers. The gA channel structure is quite rigid, independent of the lipid bilayer type, and the dimer is more rigid than the monomer.

To explore the gA orientation and dynamics in the different bilayers, we determined the average tilt (θ) and rotation (ρ) of the dimers and monomers (see definition in Fig. S2). To define ρ, the Cα atom of Trp^9 in one subunit was used as a reference atom. The θ distribution follows the hydrophobic mismatch concept (Fig. 3 *A*). That is, to maximize the hydrophobic match between the channel and the bilayer, θ decreases as the bilayer hydrophobic thickness increases: 14.5 ± 6.3° (DLPC) > 12.2 ± 6.2° (DMPC) > 9.1 ± 4.6° (DOPC) ≈ 8.9 ± 5.2° (POPC). In contrast, there are no significant differences in θ among the monomeric subunits in different lipid bilayers (Fig. 3 *B*), which float freely in one leaflet of DOPC and POPC bilayers (see below). Except in DLPC bilayers, ρ of gA dimers have a slight preference for −90°, which is the tilt direction between Trp^{13} and Trp^{15} (see Fig. S3 and Fig. S4). The ρ distributions, however, are much broader than those observed in single-pass TM α-helices (e.g., WALPs and VpuTM) (31–33) because of gA's small θ.

Knowing θ, we can compare our results with experimental data. The dynamic extent of (mis)alignment between the molecular *Z* axis and the membrane normal is characterized by the ensemble-averaged order parameter, $S_{zz} = \langle 2\cos^2(\theta) - 1\rangle/2$. S_{zz} for the gA channel backbone is 0.92–0.93 in DMPC bilayers (34–36). Fig. 3 *C* shows the S_{zz} distributions: 0.89 ± 0.09 (DLPC), 0.91 ± 0.08 (DMPC), 0.95 ± 0.05 (DOPC), and 0.94 ± 0.07 (POPC). The average S_{zz} from MD simulations in DMPC bilayers is in excellent agreement with experimental measurements. Notably, though gA channels do respond to a hydrophobic mismatch by changing their θ, the extent of the response is modest compared to those in single-pass TM α-helices (e.g., VpuTM: 35° in DLPC to 18° in DOPC and WALPs: 12° of WALP19 to 28° of WALP23 in DMPC) (31–33). The different behaviors are presumably due to the four Trp residues in each gA monomer and their strong preference to be at the bilayer's hydrophobic/hydrophilic interface (37).

To further explore the effect of hydrophobic mismatch on the channel structure, we examined the distributions of the Trp dihedral angles χ_1 and χ_2 (Fig. 4 *A* and see Fig. S5).

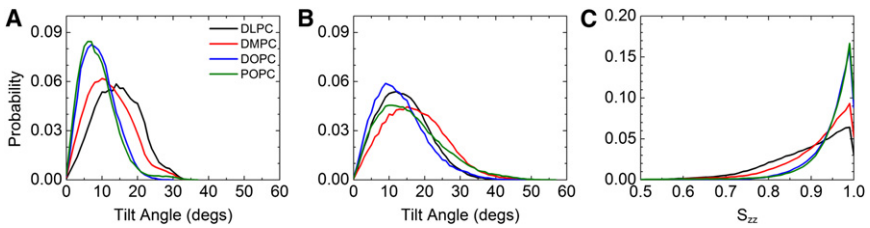

FIGURE 3 Tilt angle (θ) distributions of (*A*) a gA dimer and (*B*) a monomeric subunit in different lipid bilayers, obtained from the three independent 100-ns productions for each bilayer. (*C*) S_{zz} ($S_{zz} = \langle 2\cos^2(\theta) - 1\rangle/2$), distribution of a gA dimer in the different bilayers. The results for each system are averages over the three simulations.

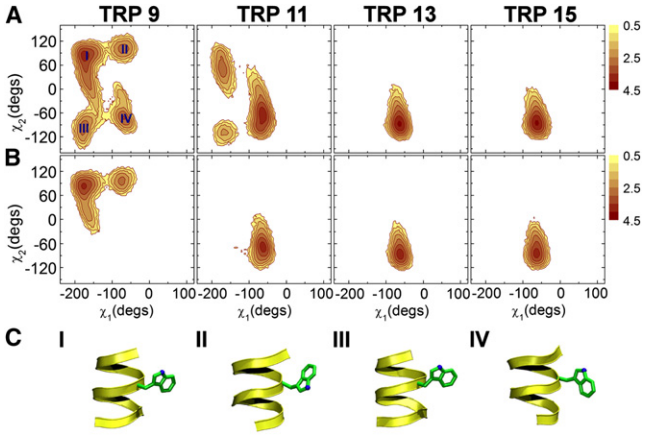

FIGURE 4 Trp dihedral angles χ_1 and χ_2 of (*A*) gA dimers and (*B*) the monomeric subunits in DOPC bilayers. The contours/colors represent the number of counts per a 5° square bin on a $\log_{10}$ scale, and are averaged over the three simulations. (*C*) Molecular representation of each Trp^9 rotamer state. (*Yellow*) gA monomer; Trp^9 for carbon atoms (*green*) and for nitrogen atoms (*blue*).

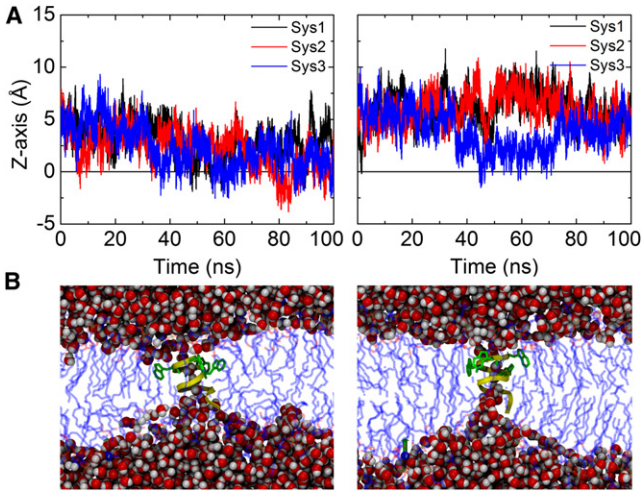

FIGURE 5 Monomeric subunits in DLPC (*left column*) and DMPC (*right column*) bilayers. (*A*) Time series of the Z coordinate of the gA monomer's COM in the bilayers. (*B*) Snapshots of water pore formation in the bilayers. (*Yellow*) gA monomeric subunit; (*green*) Trps; and (*blue*) lipid molecules. (*Spheres*) Water atoms.

Trp^{11}, Trp^{13}, and Trp^{15} have a single predominant dihedral angle ($\chi_1 \approx -60°$, $\chi_2 \approx -80°$), and the distribution of rotameric states does not vary systematically with the changes in the phospholipid acyl chain (bilayer thickness). As found previously (15,24), Trp^9 is more mobile than the other Trps, presumably because it is more deeply buried and therefore not so strongly coupled to hydrogen-bond acceptors at the bilayer/solution interface. Consistent with this interpretation, Trp^9 in the monomers (Fig. 4 *B* and see Fig. S6) is less buried and less mobile.

Despite the lower Trp^9 mobility in the monomeric subunits, the overall monomer conformations are more dynamic than the dimer conformations (see Fig. S1), as reflected in the higher RMSDs (Fig. 2 *A*), and the monomers move more freely in the bilayers. The monomeric subunits usually floated at the bilayer/solution interface (see Fig. S7 for the behavior in DOPC and POPC bilayers), reflecting fewer constraints imposed by the bilayer. The DLPC and one of DMPC systems provide notable exceptions. As shown in Fig. 5, as the monomeric subunits moved toward the bilayer center ($Z = 0$), they formed monomeric, water-permeable channels after ~40 ns. The Trps on one end of these monomeric channels remained at the hydrophobic/hydrophilic interface and pulled their surrounding lipid molecules down as the monomer moved toward the bilayer center. The formyl group made hydrogen bonds with interfacial moieties in the opposite leaflet, and the lipid bilayer close to the subunits was grossly deformed (see next section). Once formed, all pores remained stable for the remainder of the trajectory.

Both the bilayer-spanning dimers and monomers are water-permeable. To quantify the water permeability, we traced the Z coordinates of all the water molecules that visited the pore region of dimer or monomer; a complete water penetration (+1 into the $+Z$ direction and –1 into the $-Z$ direction) was recorded only if a water molecule moved from $Z = -12$ Å to 12 Å, or vice versa (see Fig. S8). Water movement in the single-filing pore can be interrupted (as indicated by the plateau regions) by EAM swing motion and K^+ binding at the channel entrances (Fig. 2 *A* and see Fig. S1 *A*).

Influence of hydrophobic mismatch on lipid structure and dynamics

The gA dimers perturb the DOPC and POPC bilayers, as evident in Fig. 1 (*top panel*). The perturbations of the DLPC and DMPC bilayers are much harder to ascertain from the figure; averaging over all equilibrated coordinate sets is required to characterize the interactions and establish differences among the lipids. The gA monomers have relatively modest effects, especially the lower leaflets, in the nonpore states (Fig. 1, *bottom panel*). To examine the hydrophobic mismatch-induced changes in lipid structure and dynamics quantitatively, we first explored the lipid distribution around the gA dimers and monomers in the different bilayers. We calculated the two-dimensional radial distribution function, $g(r)$, based on the center of mass (COM) or the choline N atoms of each lipid type, as a function of radial distance (r) from the gA center,

$$g(r) = \frac{\rho(r)}{\rho_{bulk}} = \frac{N(r, r+dr)}{2\pi r dr}\frac{1}{\rho_{bulk}}, \quad (1)$$

where $2\pi r dr$ is the area in between r and $r + dr$; $N(r,r + dr)$ is the number of lipid molecules in the area; and ρ_{bulk} is the two-dimensional density of a pure lipid bilayer. Fig. 6 and

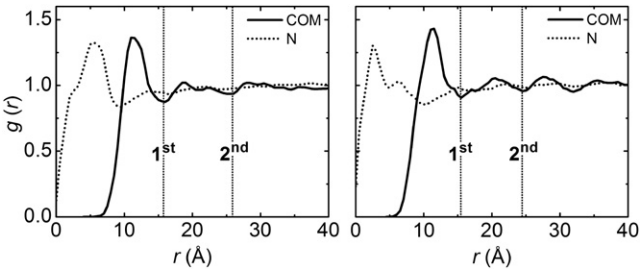

FIGURE 6 Radial distribution functions of the lipid choline N atom and the lipid COM around gA dimers (*left*) and monomeric subunits (*right*) as a function of *r* in DOPC bilayers. (*Dotted lines*) First and second shells.

Fig. S9 plot $g(r)$ for each lipid type, and Table 1 summarizes each shell size based on the COM $g(r)$ and the number of lipid molecules in each shell. There is little variation among the different lipid types. The first peak is at 11–12 Å, and there are 9–11 lipid molecules in the first shell. The $g(r)$ based on the choline N atom shows that the choline moiety in the phospholipid headgroup may interfere with gA channel function, as suggested previously (38); Fig. S10 shows examples of cholines extending over the pore entrance. Though such choline conformations could block water movement, their residence times were usually <10 ps, and there was no clear correlation between water flux and choline blocking in Fig. S8.

Knowing $g(r)$, we then could examine how lipid bilayer structure and dynamics responds to different hydrophobic mismatches by calculating the hydrophobic thickness, per-lipid surface area, compressibility, acyl chain order parameters, and lateral diffusion coefficients as functions of *r*. These are designated by the usual symbol followed by (r); e.g., the bilayer hydrophobic thickness, d_H, is commonly defined as the average distance between the acyl-chain C2 carbon atoms in both leaflets (31,39), and is written as $d_H(r)$. Similarly, the local area per lipid, area compressibility, and diffusion coefficient are denoted $A(r)$, $K_A(r)$, and $D(r)$, respectively.

The thickness profiles (Fig. 7 *A*; two-dimensional thickness profiles in Fig. S11) show both expected and surprising features. As would be expected from the gA channel structure, the two-dimensional thickness profile is radially symmetric and we observed no evidence for residual hydrophobic exposure (40), meaning that there is near-perfect hydrophobic adaptation between the channel and its surrounding phospholipids. The radially symmetric two-dimensional thickness profiles justify the construction of $d_H(r)$ plots in Fig. 7 *A*. The profiles also show a remarkable variation in thickness within the first shell, with some lipids being more extended than their neighbors. These hot spots arise from lipids with cholines interacting with the pore entrance and lipids that slide over the Trp side chains so that their carbonyl and phosphate oxygens can form hydrogen bonds with the indole NH groups. Fig. S12 shows snapshots that illustrate such interactions; Fig. S13 shows the statistical distribution of phospholipid headgroup and backbone contacts with the side chains of the gA dimer, where the lipid carbonyl and phosphate oxygens are prevalently closer to the Trp residues and the cholines tend to be prevalently closer to the Leu residues. This organization is reminiscent of that suggested by Meulendijks et al. (41), but the interactions are unlikely to be (chemically) specific in the usual sense because the gA channel function does not depend on the gA channel or phospholipid chirality (42). Moving away from the channel, $d_H(r)$ decreases within 4–5 Å from the dimer/bilayer boundary (Fig. 7 *A*). This decrease reflects, in part, the hot spots in the two-dimensional profiles (see Fig. S11), which tends to increase the bilayer thickness adjacent to the channel. Excluding the hot spots in the thickness calculations reduced the $d_H(r)$ changes from ~4 Å to ~2 Å (for DMPC, POPC, and DOPC) and from ~6 Å to ~3 Å for DLPC.

The nonmonotonic $d_H(r)$ profiles are in apparent agreement with the profile deduced by Huang (5) using the continuum theory of elastic bilayer deformations. However, the profiles differ in that the nonmonotonic behavior predicted by the continuum theory extends over much longer distances than that observed in the MD-derived profiles (see below). The $d_H(r)$ profiles in Fig. 7 *A* and Fig. S11 differ also from the profiles deduced by Helfrich and Jakobsson (6) and Nielsen et al. (8) by minimizing the deformation energy and by Lundbæk and Andersen (11) by fitting the continuum theory to the gA lifetime versus bilayer thickness data of Elliott et al. (43). These issues are explored in Fig. 8, in which we compare the $d_H(r)$ profiles from the MD simulations with those derived using the continuum elastic bilayer deformation models (5,7,9), with the slope of the bilayer/solution interface at the channel/bilayer boundary (s) chosen to be, 1), the slope from the MD profile, s_{MD}; 2), zero; and 3), the local curvature (the inverse of the

TABLE 1 Lipid shell size (first and second) and the number of lipid molecules in each shell with standard error of three systems

	Dimer (# of lipid)		Monomer (# of lipid)	
Lipid	First shell	Second shell	First shell	Second shell
DLPC	15.0 Å (9.2 ± 0.1)	21.5 Å (12.3 ± 0.2)	15.0 Å (8.5 ± 0.1)	22.5 Å (13.8 ± 0.1)
DMPC	15.0 Å (9.4 ± 0.2)	22.0 Å (13.7 ± 0.2)	14.5 Å (8.3 ± 0.4)	NA
DOPC	16.0 Å (9.2 ± 0.2)	26.0 Å (19.1 ± 0.3)	15.5 Å (8.9 ± 0.1)	24.5 Å (16.1 ± 0.3)
POPC	17.0 Å (11.2 ± 0.3)	27.5 Å (22.9 ± 0.2)	14.5 Å (7.7 ± 0.1)	NA

For the dimer, upper and lower leaflets are considered; for the monomeric subunit, only the upper one is considered.

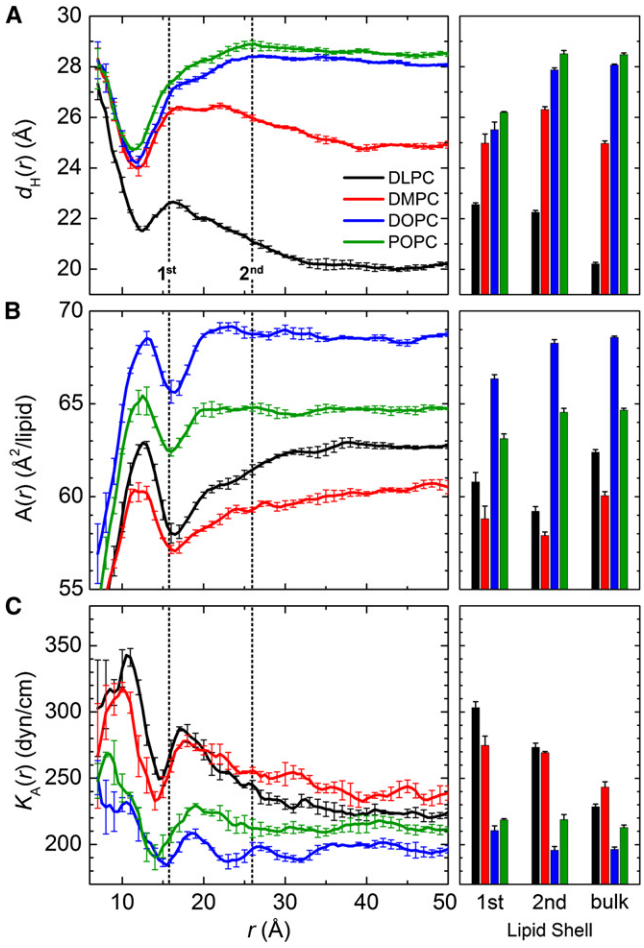

FIGURE 7 (*A*) Hydrophobic thickness profile, (*B*) area per lipid profile, and (*C*) compressibility profile as a function of r (mean ± standard error). (*Right-hand panels*) Average results for the first and second lipid shells and for the bulk. (*Dotted lines*) First and second shells.

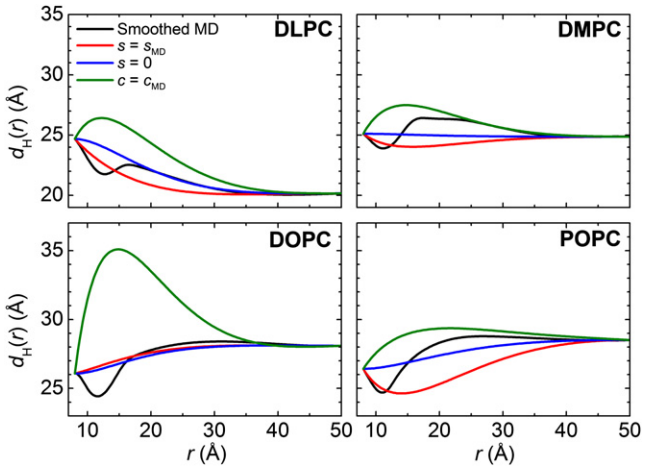

FIGURE 8 Comparison of the MD-derived deformation profiles for gA dimers in DLPC, DMPC, DOPC, and POPC bilayers with those deduced from one-dimensional continuum elastic bilayer deformation models with constant moduli (8,9,53). The lipid-protein contact boundary conditions for the continuum elastic models were chosen to be: the gradient ($s = s_{MD}$), curvature ($c = c_{MD}$) of $d_H(r)$ at the dimer/bilayer contact obtained from MD simulation, and zero gradient ($s = 0$). The MD profiles (Fig. 7 *A*) are smoothed with B-spline cubic interpolation to avoid numerical instability.

second derivative from the MD profile). None of the boundary conditions reproduces both the first valley near the protein/bilayer contact and the convergence toward the bulk value. The spatial extent of the oscillating behavior in the MD-derived $d_H(r)$ profile, and the convergence to the bulk values, is less than predicted using the analytic solution (7), even when $s = s_{MD}$. Adjusting the contact boundary condition does not appear to be sufficient to reproduce the deformation profile using the continuum elastic theory, suggesting that the deformation profile in the vicinity of the channel (within the first lipid shell) is determined by channel-lipid interactions that are not captured in the continuum elastic model (at least for gA channels). A direct calculation of the deformation energy from the MD-derived $d_H(r)$ profiles is unfortunately not trivial, as the numerical uncertainties associated with calculating the higher derivatives preclude this approach; see also Mondal et al. (40).

Except for DLPC, the $d_H(r)$ profiles close to the dimers are similar. This does not imply, however, that there is less hydrophobic adaptation in DLPC bilayers because the dimer's θ is larger in this system (see Fig. 3 *A*). In the case of DLPC (positive mismatch) and DMPC (near-match) bilayers, the perturbation extends over the first and second shells, whereas the lipid adaptation in DOPC and POPC (negative mismatch) bilayers occurs mostly within the first shell. The average DLPC bilayer thickness in the first shell is ~2 Å thicker than the bulk thickness, in general agreement with the x-ray diffraction results (44). The average DMPC bilayer thickness in the first shell is ~3 Å greater than that in the DLPC system (Fig. 7 *A*), in general agreement with Harroun et al. (44), who estimated the local thickness in the DMPC system to be 2 Å greater than in the DLPC system.

Compared to our previous study (31) showing that the free energy-minimum orientations of WALP helical peptides minimize a hydrophobic mismatch by changing θ with minimum perturbation of lipid bilayers, the gA channels in DLPC and DMPC bilayers show strong lipid adaptation. In other words, simple single-pass TM helices such as WALPs and VpuTM respond to a large hydrophobic mismatch through changes in θ, whereas the gA channels overcome the energetic penalty due to a hydrophobic mismatch by imposing changes in $d_H(r)$ with minimal changes in θ. Similar conclusions have been made for G-protein-coupled receptors (40,45).

The free-floating monomeric subunits impose fewer constraints on the bilayer, as compared to the bilayer-spanning dimers, and there is little lipid adaptation (see Fig. S14 and Fig. 7 *A*)—except when the monomeric subunits span the bilayer (Fig. 5). In this case, the bilayer-spanning inclusion is asymmetric and the deformation

profiles in the two bilayer leaflets are dissimilar (see Fig. S15). The two-dimensional thickness profiles for each leaflet and the full bilayer (Fig. S15 *A*) are radially symmetric for the monomers, justifying the construction of one-dimensional profiles (Fig. S15 *B*). In the upper leaflet, the profile displays oscillatory behavior, similar to that observed for the bilayer-spanning dimer; in the lower leaflet, the profile is monotonic. These results suggest that the deformation profiles within the first lipid shell around the bilayer-spanning dimer (Fig. 7 *A*) at least, in part, are due to lipid-tryptophan interactions.

Phospholipids are almost incompressible (46), in which case the $d_H(r)$ profiles in Fig. 7 *A* should be associated with reciprocal changes in lipid area. To explore this, we estimated the per-lipid surface area, $A(r)$, using the Voronoi tessellation approach by Pandit et al. (47). A lipid molecule was first defined by three key atoms located approximately at the hydrophobic/hydrophilic interface: the two carbonyl carbon atoms on each chain and the carbon that connects the two aliphatic chains to the chain leading to the phosphate. The gA structure was defined by the backbone heavy atoms. Delaunay triangulation was then used to determine the circumcenters of triangles that resulted in vertices for the Voronoi polygons to obtain lipid areas, and the Quickhull program (48) was used for this geometric calculation. In each bilayer type, $A(r)$ is indeed anticorrelated with $d_H(r)$ (Fig. 7 *B*). The $A(r)$ values in the bulk region agree well with per-lipid surface areas estimated in previous MD simulations (25), and lipid bilayer experiments: 63.2 ± 0.5 Å^2 (DLPC), 60.6 ± 0.5 Å^2 (DMPC), 67.4 ± 1.0 Å^2 (DOPC), and 68.3 ± 0.5 Å^2 (POPC) (49,50). Because $A(r)$ is (anti)-correlated with $d_H(r)$, the profile is not simply monotonic. Beyond the first shell, $d_H(r)$ increases gradually in the case of positive mismatch. In the case of negative mismatch, the lipid bilayer adjustment occurs within 20 Å, and one might expect $A(r)$ to be increased near the protein because of lipid compression (51). This area increment was not observed due to the local increase in $d_H(r)$.

We estimated the local lipid compressibility modulus, $K_A(r)$, assuming that $K_A(r)$ can be obtained from the per-lipid surface areas together with their fluctuations as in pure lipid bilayers (52),

$$K_A(r) = \frac{k_B T A(r)}{N\langle \delta A(r)^2 \rangle}, \quad (2)$$

where k_BT is the thermal energy and N the number of lipid molecules in a leaflet. Fig. 7 *C* shows $K_A(r)$ for each system. The compressibility moduli for the bulk ($r >$ ~30 Å) are similar to each other, 200–250 dyn/cm, and to those of pure lipid bilayers: 234 ± 23 dyn/cm (DMPC) and 237 ± 16 dyn/cm (DOPC) (53). The $K_A(r)$ values for lipids in the first shell are higher than the bulk values, indicating that the lipid acyl chains in the vicinity of the channel are harder to compress. From the calculated lipid bilayer parameters ($d_H(r)$, $A(r)$, and $K_A(r)$), we conclude that the first shell is highly perturbed because the system has to adjust to both gA-lipid interactions (hydrogen-bond formation to the indole NH groups) and hydrophobic mismatch to maintain the constant bilayer density. In the second shell, the lipids are less stressed than in the first shell, and then the perturbation decays monotonically. $A(r)$ and $K_A(r)$ in the first shell are subject to uncertainty because of the arbitrariness in defining the gA structure in the Voronoi polyhedral calculations. Nonetheless, the consistency between these quantities and $d_H(r)$, which is not calculated from Voronoi polyhedra, indicates that the Voronoi definitions are reasonable.

The hydrophobic mismatch-imposed lipid adaptation around gA channels (Fig. 7) affects acyl chain dynamics and orientation (51). The relative order of the hydrocarbon tails can be obtained from the order parameter, S_{CD},

$$S_{CD} = \frac{1}{2}\langle 3\cos^2\theta_{CH} - 1\rangle, \quad (3)$$

where θ_{CH} is the angle between the CH bond vector and the bilayer normal; S_{CD} defined in this way can be directly compared with the order parameter measured by deuterium NMR, and is therefore denoted as the deuterium order parameter. Fig. 9 compares S_{CD} in each shell and includes available experimental measurements (54,55). As in previous studies (14), DLPC and DMPC bilayers (Fig. 9, *upper row*) show higher S_{CD} in the first and second shell than in the bulk lipids due to the chain ordering induced by the local increase in $d_H(r)$ (Fig. 7 *A*) together with the decrease in $A(r)$ (Fig. 7 *B*). In contrast, in the first shell of

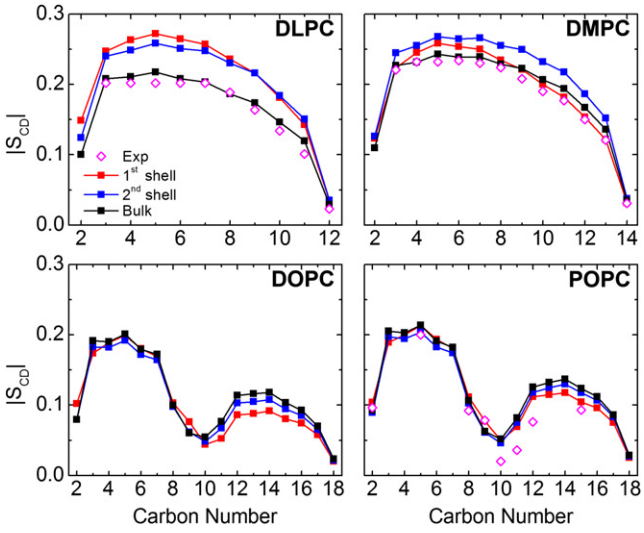

FIGURE 9 ^{2}H order parameter of DLPC, DMPC, DOPC, and POPC (oleoyl chain in the C2 glycerol backbone carbon) bilayers for the first and second lipid shells and bulk lipid (*red*, first shell; *blue*, second shell; *black*, bulk; *magenta diamond*, experimental results).

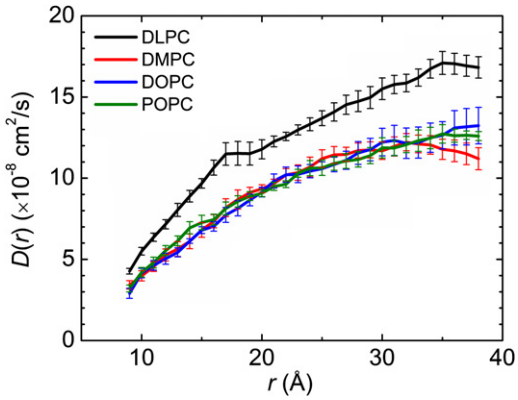

FIGURE 10 Lipid lateral diffusion coefficient as a function of r (mean ± standard error) for each bilayer system.

DOPC and POPC bilayers (Fig. 9, *lower row*), which is more compressed than the bulk lipids due to negative mismatch, S_{CD} is less than in bulk.

To further explore how protein-lipid interactions affect lipid dynamics, we investigated the influence of protein-lipid interactions on lipid diffusion. The lateral diffusion coefficient, $D(r)$, was calculated on a grid in the XY plane around the gA dimer from the lateral mean-squared displacement of each lipid COM, $\Delta x(t) = x(t + \Delta t) - x(t)$ (56,57):

$$D(r) = \frac{\left\langle [\Delta x(t) - \langle \Delta x(t) \rangle]^2 + [\Delta y(t) - \langle \Delta y(t) \rangle]^2 \right\rangle}{4\Delta t}. \quad (4)$$

At each grid point (grid spacing = 1.0 Å), $D(r)$ was calculated with Δt = 10 ns; the calculated bulk values in the gA systems are in reasonable agreement with diffusion coefficients in pure lipid bilayers with an average error of 15%. Fig. 10 and Fig. S16 show the one-dimensional and two-dimensional $D(r)$ distributions for each lipid bilayer system. $D(r)$ in the first and second shells are lower than in the bulk, and show a weak correlation with the profiles for $d_H(r)$, $A(r)$, and $K_A(r)$ (Fig. 7). Because DMPC, DOPC, and POPC bilayers have the same headgroup and very similar $D(r)$ profiles (~13.0 × 10^{-8} cm^2/s in the bulk), the levels of acyl chain saturation, hydrophobic thickness, and hydrophobic mismatch do not seem to be major determinants of $D(r)$. $D(r)$ values in DLPC bilayers are much larger than for the other systems, but the relative changes in $D(r)$ between the first shell and the plateau region (at ~40 Å) vary little among the different systems: 2.32 (DLPC), 2.31 (DMPC), 2.41 (DOPC), and 2.10 (POPC). We conclude that there is nothing special about the lipid adaptation in DLPC bilayers that can explain the different $D(r)$ profile.

CONCLUSIONS

Molecular dynamics simulations of gA dimers and monomers in all-atom DLPC, DMPC, DOPC, and POPC bilayers reveal a range of responses to different peptide-bilayer hydrophobic mismatches. The structure of the gA dimer is largely unaffected by changes in lipid bilayer composition (thickness), and its tilt varies from 14° in DLPC, the thinnest bilayer, to 9° in DOPC. This 5° variation in tilt is less than the 16~17° difference deduced for single-pass TM α-helices in bilayers formed by the same lipids (33) or in similar mismatch conditions (31). That is, the lipid bilayer adapts to the gA, whereas single-pass TM α-helices such as WALPs and VpuTM adapt to the lipid bilayer. The monomeric gA subunits retain their β-helical conformation for the 100-ns simulations. They float in a single leaflet in DOPC and POPC bilayers, but can form water-permeable bilayer-spanning channels in DLPC and DMPC bilayers.

The bilayer structure and dynamics in the first lipid shell around gA dimers reflect both the channel-bilayer mismatch and hydrogen-bond formation between the phospholipid carbonyl and phosphate oxygens and the indole NH groups. Our results provide support for the importance of hydrophobic adaptation between integral membrane proteins and their host bilayer, but demonstrate also an unexpected feature, namely that a lipid may extend out of the bilayer so that its choline group can interact with the pore entrance as in the case of gA channels. The radial dependence of hydrophobic thickness, lipid area, and bilayer compressibility vary nonmonotonically over the first lipid shell around the channel and reach their bulk values in the second shell in DOPC and POPC bilayers and in the third shell in DLPC and DMPC bilayers. Order parameters and diffusion coefficients also differ for lipids in the first and second shells and the bulk. Reflecting the different order parameters, the local compressibility moduli in the vicinity of the channel are higher than the bulk values. This supports Partenskii and Jordan's conjecture (10) that the channel alters the local lipid dynamics—and thus the local moduli—beyond what would be predicted from a simple mismatch model. It also provides a rationale for why Lundbæk and Andersen (11) found that the experimental gA single-channel lifetime versus bilayer thickness relation could be fit by the continuum description (with constant moduli) only when using a phenomenological spring coefficient that was threefold larger than the value predicted using equilibrium theory and assuming no constraints on lipid structure and dynamics (apart from that imposed by the hydrophobic mismatch).

The MD-derived deformation profiles differ from those predicted using the simple continuum theory of bilayer deformations, which is likely to reflect a combination of hydrogen bond-stabilized phospholipid-indole NH interactions, choline-pore entrance interactions (which causes the lipid to extend out of the bilayer), and the radial variation in the elastic moduli. The increased local moduli, taken together with the complex deformation profiles, indicate that the bilayer deformation energies, i.e., the energetic cost of hydrophobic mismatch-induced bilayer deformations, will

be larger than predicted using the simple continuum description (assuming constant moduli), which has implications for evaluating the energetic coupling between membrane proteins and their host bilayer.

SUPPORTING MATERIAL

One table and 16 figures are available at http://www.biophysj.org/biophysj/supplemental/S0006-3495(12)00324-4.

This work was supported in part by the National Science Foundation (MCB-0918374 to W.I.); TeraGrid resources were provided by Purdue University (National Science Foundation. OCI-0503992 to W.I.), the National Institutes of Health (GM021342 to O.S.A.), and the Intramural Research Program of the National Institutes of Health, National Heart, Lung and Blood Institute (to R.W.P.).

REFERENCES

1. Andersen, O. S., and R. E. Koeppe, II. 2007. Bilayer thickness and membrane protein function: an energetic perspective. *Annu. Rev. Biophys. Biomol. Struct.* 36:107–130.
2. Southall, N. T., and K. A. Dill. 2000. The mechanism of hydrophobic solvation depends on solute radius. *J. Phys. Chem. B.* 104:1326–1331.
3. Lundbæk, J. A., S. A. Collingwood, …, O. S. Andersen. 2010. Lipid bilayer regulation of membrane protein function: gramicidin channels as molecular force probes. *J. R. Soc. Interface.* 7:373–395.
4. Mouritsen, O. G., and M. Bloom. 1984. Mattress model of lipid-protein interactions in membranes. *Biophys. J.* 46:141–153.
5. Huang, H. W. 1986. Deformation free energy of bilayer membrane and its effect on gramicidin channel lifetime. *Biophys. J.* 50:1061–1070.
6. Helfrich, P., and E. Jakobsson. 1990. Calculation of deformation energies and conformations in lipid membranes containing gramicidin channels. *Biophys. J.* 57:1075–1084.
7. Aranda-Espinoza, H., A. Berman, …, S. Safran. 1996. Interaction between inclusions embedded in membranes. *Biophys. J.* 71:648–656.
8. Nielsen, C., M. Goulian, and O. S. Andersen. 1998. Energetics of inclusion-induced bilayer deformations. *Biophys. J.* 74:1966–1983.
9. Nielsen, C., and O. S. Andersen. 2000. Inclusion-induced bilayer deformations: effects of monolayer equilibrium curvature. *Biophys. J.* 79:2583–2604.
10. Partenskii, M. B., and P. C. Jordan. 2002. Membrane deformation and the elastic energy of insertion: perturbation of membrane elastic constants due to peptide insertion. *J. Chem. Phys.* 117:10768–10776.
11. Lundbæk, J. A., and O. S. Andersen. 1999. Spring constants for channel-induced lipid bilayer deformations. Estimates using gramicidin channels. *Biophys. J.* 76:889–895.
12. Goulian, M., O. N. Mesquita, …, A. Libchaber. 1998. Gramicidin channel kinetics under tension. *Biophys. J.* 74:328–337.
13. Ingólfsson, H. I., and O. S. Andersen. 2010. Screening for small molecules' bilayer-modifying potential using a gramicidin-based fluorescence assay. *Assay Drug Dev. Technol.* 8:427–436.
14. Chiu, S.-W., S. Subramaniam, and E. Jakobsson. 1999. Simulation study of a gramicidin/lipid bilayer system in excess water and lipid. I. Structure of the molecular complex. *Biophys. J.* 76:1929–1938.
15. Allen, T. W., O. S. Andersen, and B. Roux. 2003. Structure of gramicidin a in a lipid bilayer environment determined using molecular dynamics simulations and solid-state NMR data. *J. Am. Chem. Soc.* 125:9868–9877.
16. Jo, S., T. Kim, and W. Im. 2007. Automated builder and database of protein/membrane complexes for molecular dynamics simulations. *PLoS ONE.* 2:e880.
17. Jo, S., J. B. Lim, …, W. Im. 2009. CHARMM-GUI Membrane Builder for mixed bilayers and its application to yeast membranes. *Biophys. J.* 97:50–58.
18. Jo, S., T. Kim, …, W. Im. 2008. CHARMM-GUI: a web-based graphical user interface for CHARMM. *J. Comput. Chem.* 29:1859–1865.
19. Townsley, L. E., W. A. Tucker, …, J. F. Hinton. 2001. Structures of gramicidins A, B, and C incorporated into sodium dodecyl sulfate micelles. *Biochemistry.* 40:11676–11686.
20. Feller, S. E., Y. Zhang, and R. W. Pastor. 1995. Computer simulation of liquid/liquid interfaces. II. Surface tension-area dependence of a bilayer and monolayer. *J. Chem. Phys.* 103:10267–10276.
21. Brooks, B. R., C. L. Brooks, III, …, M. Karplus. 2009. CHARMM: the biomolecular simulation program. *J. Comput. Chem.* 30:1545–1614.
22. MacKerell, Jr., A. D., D. Bashford, …, M. Karplus. 1998. All-atom empirical potential for molecular modeling and dynamics studies of proteins. *J. Phys. Chem. B.* 102:3586–3616.
23. Mackerell, Jr., A. D., M. Feig, and C. L. Brooks, III. 2004. Extending the treatment of backbone energetics in protein force fields: limitations of gas-phase quantum mechanics in reproducing protein conformational distributions in molecular dynamics simulations. *J. Comput. Chem.* 25:1400–1415.
24. Ingólfsson, H. I., Y. Li, …, O. S. Andersen. 2011. Gramicidin A backbone and side chain dynamics evaluated by molecular dynamics simulations and nuclear magnetic resonance experiments. I: Molecular dynamics simulations. *J. Phys. Chem. B.* 115:7417–7426.
25. Klauda, J. B., R. M. Venable, …, R. W. Pastor. 2010. Update of the CHARMM all-atom additive force field for lipids: validation on six lipid types. *J. Phys. Chem. B.* 114:7830–7843.
26. Jorgensen, W. L., J. Chandrasekhar, …, M. L. Klein. 1983. Comparison of simple potential functions for simulating liquid water. *J. Chem. Phys.* 79:926–935.
27. Ryckaert, J.-P., G. Ciccotti, and H. J. C. Berendsen. 1977. Numerical integration of the Cartesian equations of motion of a system with constraints: molecular dynamics of *n*-alkanes. *J. Comput. Phys.* 23:327–341.
28. Steinbach, P. J., and B. R. Brooks. 1994. New spherical-cutoff methods for long-range forces in macromolecular simulation. *J. Comput. Chem.* 15:667–683.
29. Essmann, U., L. Perera, …, L. G. Pedersen. 1995. A smooth particle mesh Ewald potential. *J. Chem. Phys.* 103:8577–8592.
30. Katsaras, J., R. S. Prosser, …, J. H. Davis. 1992. Constant helical pitch of the gramicidin channel in phospholipid bilayers. *Biophys. J.* 61:827–830.
31. Kim, T., and W. Im. 2010. Revisiting hydrophobic mismatch with free energy simulation studies of transmembrane helix tilt and rotation. *Biophys. J.* 99:175–183.
32. Kim, T., S. Jo, and W. Im. 2011. Solid-state NMR ensemble dynamics as a mediator between experiment and simulation. *Biophys. J.* 100: 2922–2928.
33. Jo, S., and W. Im. 2011. Transmembrane helix orientation and dynamics: insights from ensemble dynamics with solid-state NMR observables. *Biophys. J.* 100:2913–2921.
34. Prosser, R. S., J. H. Davis, …, M. A. Lindorfer. 1991. ^{2}H nuclear magnetic resonance of the gramicidin A backbone in a phospholipid bilayer. *Biochemistry.* 30:4687–4696.
35. Killian, J. A., M. J. Taylor, and R. E. Koeppe, II. 1992. Orientation of the valine-1 side chain of the gramicidin transmembrane channel and implications for channel functioning. A ^{2}H NMR study. *Biochemistry.* 31:11283–11290.
36. Pulay, P., E. M. Scherer, …, R. E. Koeppe, II. 2005. Importance of tensor asymmetry for the analysis of ^{2}H NMR spectra from deuterated aromatic rings. *J. Am. Chem. Soc.* 127:17488–17493.
37. Lee, J., and W. Im. 2008. Transmembrane helix tilting: insights from calculating the potential of mean force. *Phys. Rev. Lett.* 100:018103.
38. Allen, T. W., O. S. Andersen, and B. Roux. 2006. Ion permeation through a narrow channel: using gramicidin to ascertain all-atom

molecular dynamics potential of mean force methodology and biomolecular force fields. *Biophys. J.* 90:3447–3468.

39. de Planque, M. R. R., and J. A. Killian. 2003. Protein-lipid interactions studied with designed transmembrane peptides: role of hydrophobic matching and interfacial anchoring. *Mol. Membr. Biol.* 20:271–284 (Review).
40. Mondal, S., G. Khelashvili, …, H. Weinstein. 2011. Quantitative modeling of membrane deformations by multihelical membrane proteins: application to G-protein coupled receptors. *Biophys. J.* 101:2092–2101.
41. Meulendijks, G. H. W. M., T. Sonderkamp, …, H. M. Buck. 1989. The different influences of ether and ester phospholipids on the conformation of gramicidin A. A molecular modeling study. *Biochim. Biophys. Acta.* 979:321–330.
42. Providence, L. L., O. S. Andersen, …, R. Bittman. 1995. Gramicidin channel function does not depend on phospholipid chirality. *Biochemistry.* 34:16404–16411.
43. Elliott, J. R., D. Needham, …, D. A. Haydon. 1983. The effects of bilayer thickness and tension on gramicidin single-channel lifetime. *Biochim. Biophys. Acta.* 735:95–103.
44. Harroun, T. A., W. T. Heller, …, H. W. Huang. 1999. Experimental evidence for hydrophobic matching and membrane-mediated interactions in lipid bilayers containing gramicidin. *Biophys. J.* 76:937–945.
45. Cordomí, A., and J. J. Perez. 2007. Molecular dynamics simulations of rhodopsin in different one-component lipid bilayers. *J. Phys. Chem. B.* 111:7052–7063.
46. Evans, E. A., and R. M. Hochmuth. 1978. Mechano-chemical properties of membranes. *In* Current Topic in Membranes and Transport. A. Kleinzeller and F. Bronner, editors. Academic Press, New York. 1–64.
47. Pandit, S. A., S. Vasudevan, …, H. L. Scott. 2004. Sphingomyelin-cholesterol domains in phospholipid membranes: atomistic simulation. *Biophys. J.* 87:1092–1100.
48. Barber, C. B., D. P. Dobkin, and H. Huhdanpaa. 1996. The Quickhull algorithm for convex hulls. *ACM Trans. Math. Softw.* 22:469–483.
49. Kučerka, N., Y. Liu, …, J. F. Nagle. 2005. Structure of fully hydrated fluid phase DMPC and DLPC lipid bilayers using x-ray scattering from oriented multilamellar arrays and from unilamellar vesicles. *Biophys. J.* 88:2626–2637.
50. Kučerka, N., S. Tristram-Nagle, and J. F. Nagle. 2005. Structure of fully hydrated fluid phase lipid bilayers with monounsaturated chains. *J. Membr. Biol.* 208:193–202.
51. Fattal, D. R., and A. Ben-Shaul. 1993. A molecular model for lipid-protein interaction in membranes: the role of hydrophobic mismatch. *Biophys. J.* 65:1795–1809.
52. Feller, S. E., and R. W. Pastor. 1999. Constant surface tension simulations of lipid bilayers: the sensitivity of surface areas and compressibilities. *J. Chem. Phys.* 111:1281–1287.
53. Rawicz, W., K. C. Olbrich, …, E. Evans. 2000. Effect of chain length and unsaturation on elasticity of lipid bilayers. *Biophys. J.* 79:3 28–339.
54. Perly, B., I. C. P. Smith, and H. C. Jarrell. 1985. Acyl chain dynamics of phosphatidylethanolamines containing oleic acid and dihydrosterculic acid: ^{2}H NMR relaxation studies. *Biochemistry.* 24:4659–4665.
55. Douliez, J. P., A. Léonard, and E. J. Dufourc. 1995. Restatement of order parameters in biomembranes: calculation of C-C bond order parameters from C-D quadrupolar splittings. *Biophys. J.* 68:1727–1739.
56. Im, W., and B. Roux. 2002. Ions and counterions in a biological channel: a molecular dynamics simulation of OmpF porin from *Escherichia coli* in an explicit membrane with 1 M KCl aqueous salt solution. *J. Mol. Biol.* 319:1177–1197.
57. Rui, H., K. I. Lee, …, W. Im. 2011. Molecular dynamics studies of ion permeation in VDAC. *Biophys. J.* 100:602–610.